A Conformal, Fully-Conservative Approach for Predicting Blast Effects on Ground Vehicles

P. Ivancic, **J.M. Janus,** **E. Luke,** **D. Thompson,** **R. Weed**

pri4@msstate.edu mark@cavs.msstate.edu luke@cse.msstate.edu dst@cavs.msstate.edu rweed@cavs.msstate.edu

Mississippi State University, Center for Advanced Vehicular Systems
Mississippi State, MS
USA

J. Kang
Tank Automotive Research, Development, and Engineering Center (TARDEC)
Warren, MI
USA

jian.kang@us.army.mil

ABSTRACT

A new blast code, Loci/BLAST, has been coupled with the commercial structural dynamics package LS-DYNA to provide a fully-coupled simulation strategy for predicting the effects of blast on a ground vehicle. Loci/BLAST is a fully-conservative, computational fluid dynamics code with the capability to model soil and blast using a multi-species formulation with advanced equations of state. The two-way coupling between Loci/BLAST and LS-DYNA provides a robust mechanism for predicting the blast-induced deformation of structural elements with no topology changes. The efficacy of the resulting software is demonstrated by comparisons of predicted deformations for a constrained plate with experimental data. Results are also presented for a notional hull subjected to the effects of detonation of a buried IED.

1.0 INTRODUCTION

Predicting the effects of a blast on a vehicle and its occupants due to the detonation of an improvised explosive device (IED) is a challenging task. In addition to the effects of the blast, the effects of soil, which could have a high water content, must also be included. An attractive strategy, which is much less costly than experimental approaches, is to employ numerical simulations to predict these complex interactions. The fidelity of the numerical simulations can vary from empirical models to hydrocode simulations to decoupled Computational Fluid Dynamics (CFD) and Computational Structural Dynamics (CSD) simulations to fully-coupled fluid-structure interaction (FSI) simulations.

There are two widely used, candidate methodologies for blast simulations: 1) Lagrangian methods or 2) Eulerian methods. Lagrangian methods simulate material deformations directly by coupling the deformation of the material with movement of the discrete mesh. These methods are usually based on a finite-element formulation and have proven to be both robust and efficient. For highly plastic or fluid flow problems, they are subject to mesh tangling that can lead to issues with both accuracy and robustness. In the case of soil in close proximity to an explosive event, the soil undergoes severe deformations that can present challenges for a Lagrangian method. In addition, material and energy leakage are problems associated with Lagrangian simulation methodologies.

UNCLASSIFED: DISTRIBUTION A.
APPROVED FOR PUBLIC RELEASE

Report Documentation Page

Form Approved
OMB No. 0704-0188

1. REPORT DATE	2. REPORT TYPE	3. DATES COVERED
09 FEB 2014	**Journal Article**	**13-03-2013 to 20-01-2014**

4. TITLE AND SUBTITLE
A Conformal, Fully-Conservative Approach for Predicting Blast Effects on Ground Vehicles

5a. CONTRACT NUMBER
W56HZV-08-C-0236

5b. GRANT NUMBER

5c. PROGRAM ELEMENT NUMBER

6. AUTHOR(S)
J Kang; J Janus; E Luke; D Thompson; R Weed

5d. PROJECT NUMBER

5e. TASK NUMBER

5f. WORK UNIT NUMBER

7. PERFORMING ORGANIZATION NAME(S) AND ADDRESS(ES)
Mississippi State University,Center for Advanced Vehicular Systems,200 Research Blvd,Starkville,MS,39759

8. PERFORMING ORGANIZATION REPORT NUMBER
; #24469

9. SPONSORING/MONITORING AGENCY NAME(S) AND ADDRESS(ES)
U.S. Army TARDEC, 6501 East Eleven Mile Rd, Warren, Mi, 48397-5000

10. SPONSOR/MONITOR'S ACRONYM(S)
TARDEC

11. SPONSOR/MONITOR'S REPORT NUMBER(S)
#24469

12. DISTRIBUTION/AVAILABILITY STATEMENT
Approved for public release; distribution unlimited

13. SUPPLEMENTARY NOTES
This material is based on work supported by the U.S. Army TACOM Life Cycle Command under Contract No. W56HZV-08-C-0236, through a subcontract with Mississippi State University, and was performed for the Simulation Based Reliability and Safety (SimBRS) research program. Any opinions, finding and conclusions or recommendations in this material are those of the author(s) and do not necessarily reflect the views of the U.S. Army TACOM Life Cycle Command.

14. ABSTRACT
A new blast code, Loci/BLAST, has been coupled with the commercial structural dynamics package LS-DYNA to provide a fully-coupled simulation strategy for predicting the effects of blast on a ground vehicle. Loci/BLAST is a fully-conservative, computational fluid dynamics code with the capability to model soil and blast using a multispecies formulation with advanced equations of state. The two-way coupling between Loci/BLAST and LS-DYNA provides a robust mechanism for predicting the blast-induced deformation of structural elements with no topology changes. The efficacy of the resulting software is demonstrated by comparisons of predicted deformations for a constrained plate with experimental data. Results are also presented for a notional hull subjected to the effects of detonation of a buried IED.

15. SUBJECT TERMS

16. SECURITY CLASSIFICATION OF:			17. LIMITATION OF ABSTRACT	18. NUMBER OF PAGES	19a. NAME OF RESPONSIBLE PERSON
a. REPORT	b. ABSTRACT	c. THIS PAGE			
unclassified	**unclassified**	**unclassified**	**Public Release**	**16**	

In contrast, an Eulerian formulation keeps the mesh fixed and allows material to convect through it thereby obviating issues associated with mesh tangling. Further, Eulerian methods are conservative by design. One disadvantage of Eulerian techniques is that they have less fidelity in capturing material interfaces due to diffusion. However, for cases that involve blast-soil interactions, the soil interface is unlikely to remain sharply defined and such a compromise is reasonable.

In this paper, we describe a simulation strategy that is based on a conformal coupling between Loci/BLAST [1-3], which is an Eulerian, CFD-based blast code, and LS-DYNA [4], which is a commercial, Lagrangian-based CSD code. First, the basic algorithm employed in Loci/BLAST is described. Then, the algorithm employed to transfer loads between the blast simulation and the CSD simulation is described. Results predicted for a simple, constrained plate are compared with experimental data [5]. Finally, predictions for the TARDEC generic hull [6] are then presented.

2.0 BACKGROUND

The literature contains numerous examples of simulations to predict blast effects on vehicles. This review, which is not intended to be exhaustive, highlights a few of these efforts that employ a coupled Eulerian-Lagrangian strategy similar to the approach described in this paper.

Tai *et al*. [7] investigated the interactions and impact effect between air-blast waves and an armored vehicle. The geometry consisted of a simplified model of a six-wheeled armored tank, including the muzzle, turret, wheels, and hull. The decoupled inviscid CFD simulations (i.e. assuming a rigid vehicle) were used to examine the pressure variation and shock wave interaction with the vehicle. Silver [8] used a commercial CFD code to predict the overpressure of a large caliber gun mounted on a simplified, rigid tank geometry. Similarly, Kim and Han [9] used a commercial CFD code and a structural response code (GUNBLAST) to predict the response of and damage to an aircraft wing and equipment mounted in the aircraft that were subjected to repetitive blast waves from a gun mounted on the aircraft.

Lottati *et al*. [10] used a coupled CFD/CSD approach to design a blast deflector to improve the survivability of a tactical vehicle subject to mine blasts at different locations under the crew cab and wheels. The pressures were calculated using the inviscid AUGUST-3D CFD code. The assessment of the structural response to the blast load was computed using the DYNA CSD code. A simplified geometry model of the eight-wheeled vehicle included the cab, body, frame, wheels, transmission, and axles.

Fairlie and Bergeron [11] used a coupled Euler-Lagrangian approach with the AUTODYN hydrocode to perform mine blast loading simulations to assess blast effects on a light armor vehicle. The blast simulations demonstrated both above ground (air blast) and buried charges and were used to extract local velocity measurements from various parts of the vehicle. For these simulations, a complete model of the vehicle structure, suspension system, and wheels was created in order to ensure a realistic response to a mine detonation under one of the vehicle wheels. The model also included other bulky and heavy components such as the engine gearbox, differentials, leaf springs, axles, shock absorbers, wheels, and tires.

Grujicic *et al*. [12] performed numerical simulations demonstrating the effects of a mine blast on a commercial truck. The simulations modeled the interactions between the detonation-products/soil ejecta resulting from the explosion of a shallow-buried mine and a Ford F800 single-unit commercial truck. The simulations were performed using the Eulerian-Lagrangian coupling options with the AUTODYN hydrocode. An especially detailed geometric model of the truck was used. The results showed that: 1) the kinematic response of the vehicle to a landmine detonation and the amount of blast momentum transfer is sensitive to the proportion of

water in the sand into which the landmine is buried – for saturated sand, the tunneling-effect gives rise to localized damage while for dry sand, the damage is spread out over a larger area – and 2) the presence of frequency components in the initial blast-loading impulse that match the vehicle's natural frequency plays a significant role in the kinematic response and damage of the vehicle.

Grujicic *et al*. [13] also conducted simulations to determine the survivability of a 1994 Chevrolet C1500 commercial pick-up truck subjected to the detonation of landmines buried in different soil types. These simulations were also performed using the Eulerian-Lagrangian coupling options with the AUTODYN hydrocode. Again, a very detailed model of the pick-up truck was used. The results demonstrated that the soil type and moisture content affect both the extent and spatial distribution of the damage and the kinematic response of the vehicle and that the blast load contains minimal low-frequency content and therefore does not provoke a whole-vehicle resonance response when subjected to the mine-detonation loading.

Fallet [14] conducted a simulation of an explosion of a buried landmine under the front wheel of a civilian pickup truck. The simulation was performed using a coupled Eulerian-Lagrangian approach with the HyperWorks RADIOSS model. The geometry included the complete vehicle, specifically a detailed model of the cabin, tires, wheels, suspension, and underbody. The results of the simulation were used to determine where to reinforce the vehicle structure with armor plates to limit blast penetration into the vehicle. It was also used to design energy absorbers for the vehicle seats to limit the acceleration level on the passenger.

3.0 METHODOLOGY

3.1 Blast and Soil Modeling

The numerical methods employed to simulate the blast and blast/soil interaction are described in detail in Thompson *et al*. [1-3]. Loci/BLAST is a relatively new blast code [1,2,3] that extends the capabilities of the Loci/CHEM flow solver [15] to model blast events through the addition of advanced equations of state (EoS), such as the Jones-Wilkins-Lee (JWL) EoS [16], to model explosive material and soil. Loci/CHEM is a full-featured flow solver that has undergone extensive verification and validation and has been demonstrated to scale efficiently to thousands of processors. Loci/BLAST has successfully been applied to modeling blast-soil interactions such as the simulation of landmines buried in sand, with and without moisture. Loci/CHEM and Loci/BLAST are both based on the Loci software framework [17], which simplifies the development of complex multi-physics high resolution numerical models.

3.1.1 Governing Equations

The governing equations for the soil-blast model are those of a multicomponent inviscid flow assuming thermal, pressure, and velocity equilibrium between all materials in any given region in space. These equations are described by the conservation of component mass, momentum, and energy, which are given by

$$\frac{\partial \rho_i}{\partial t} + \nabla \bullet \left(\rho_i \vec{u}\right) = 0, \forall i \in \left\{1 \ldots NS\right\} \tag{1}$$

$$\frac{\partial \rho \vec{u}}{\partial t} + \nabla \bullet \left(\rho \vec{u} \vec{u}\right) = \nabla p \tag{2}$$

$$\frac{\partial \rho e_0}{\partial t} + \nabla \bullet \left[(\rho e_0 + p)\vec{u} \right] = 0 . \tag{3}$$

Here, ρ_i is the component density of material *i*, $\vec{u}$ is the material velocity vector, p is the pressure of the component mixture. Note that *NS* is the number of component species and the overall material density at any point is given by $\rho = \sum_{i=1}^{NS} \rho_i$. The total energy per unit mass, e_0, is the sum of the fluid kinetic energy and internal energy given by the expression

$$e_0 = \frac{1}{2}\vec{u} \cdot \vec{u} + e_{\text{internal}} . \tag{4}$$

These equations are closed by a multicomponent EoS that relates pressure to the material densities of the components and the internal energy as represented by $p = p(\rho_1, \rho_2, \cdots, \rho_{NS}, e_{\text{internal}})$. The formulation of this EoS is central to the soil and blast gas models, which are derived from a mixture rule that combines single component equations of state for each material, assuming pressure and thermal equilibrium.

3.1.2 Multicomponent EoS for Blast Modeling

To support non-ideal equations of state for blast modelling, a robust density-energy query capability is needed. The resulting mixing rule assumes that the materials are immiscible and are in mechanical (pressure) and thermal equilibrium. In this mixing rule, it is assumed that the mixture of species equations of state which define pressure as a function of density and temperature. Using the immiscible assumption, we find the volume of the mixture is the sum of the volume occupied by each species, or

$$\frac{1}{\rho} = \sum_{i=1}^{NS} \frac{Y_i}{\rho_i^*} , \tag{5}$$

where Y_i is the species mass fraction and ρ_i^* is the density of a pure material *i* at a given temperature and pressure as given by

$$p = p_i(\rho_i^*, T) \; \forall \; i \in [1 \ldots NS], \tag{6}$$

where $p_i(\rho_i^*, T)$ is the EoS for species *i*, and *p* is the system pressure. The energy of the mixture is given by the mass averaged species energies, as in

$$e = \sum_{i=1}^{NS} Y_i e_i(T, \rho_i^*), \tag{7}$$

where the species energy equation is given by

$$e_i(T, \rho_i^*) = e_{f,i} + \int_{T_o}^{T} c_{v,i}(\tau) d\tau + \left[e_i(T, \rho_i^*) - e_i(T)_{pg} \right]. \tag{8}$$

The last term in this expression is the departure function that accounts for the effects of non-ideality in the EoS.

Note that equation (8) is simply a trivial regrouping of the energy components that allows us to view the energy of a species as a division of thermally perfect and thermally imperfect components. Thus the departure function is viewed as the deviation of the energy equation from a thermally perfect gas and can be computed using

$$\left[e_i\left(T,\rho_i^*\right)-e_i\left(T\right)_{pg}\right]=\int_0^{\rho_i^*}\left[p-T\frac{\partial p\left(\rho_i^*,T\right)}{\partial T}\right]\frac{d\rho_i^*}{\rho_i^{*2}}. \tag{9}$$

Equations (5), (6), and (7) describe *NS*+2 nonlinear equations and *NS*+4 unknowns (the unknowns are the species specific volumes $1/\rho_i^*$ and the thermodynamic variables *P*, *T*, ρ, and *e*). Given any two thermodynamic state variables, this system of equations can be solved to find the remaining thermodynamic variables along with the specific volumes implied by the species pure substance densities ρ_i^*. Due to the inherent non-linearities in these equations, robustly solving for the thermodynamic state, given the fluid density and energy (as will be required by an explicit time integrator), can be a significant challenge. The most straightforward approach is to use a multi-dimensional Newton method. However, when the initial guess is far away from the final solution, it can be difficult to reliably converge to a solution. We have developed an alternative approach that is robust, but perhaps with a sacrifice in computational efficiency.

To obtain a robust solution to the above non-linear equations, it can be observed that if the problem is cast in terms of pressure and temperature instead of density and energy, the pressure equation, i.e., equation (6), decouples and *NS* non-linear scalar equations must be solved. Since non-linear root finding for scalar equations can be made robust using root bracketing techniques, a pressure-temperature query has a very robust solution. This observation can be used to implement an indirect procedure that provides a robust density-energy Eos query. First, a robust density-temperature query can be obtained by performing a bracketed-scalar solve for the pressure. This iterative solve can utilize the robust pressure-temperature query; in addition, it is expected that pressure will increase monotonically with temperature. Finally, given a robust density-temperature query, a robust density-energy query can be formulated by solving for the temperature that gives the specified energy. All of these queries are solved using a bracketed Newton method whereby the values that bracket a solution are identified. If the Newton method overshoots the bracket, the robust bisection method is utilized for that step. The resulting EoS query evaluator has been shown to be robust in practice. A variety of species equations of state have been implemented in Loci/BLAST including a perfect gas, a density-temperature form of the JWL EoS for the explosive gas [16], a linear barytropic EoS for an elastic solid (explosive and soil), and a Tait EoS for liquid water [18].

3.1.3 Prescribed Burn Model

A prescribed burn capability is used to simulate the propagation of the detonation front through the explosive material. The current model assumes that the detonation is initiated from a single point and that there are no obstructions to the detonation front. In the prescribed explosive burn methodology, the initiation point and a detonation velocity are provided by the user. The explosive burn is accomplished by converting the solid explosive material into the corresponding gas material as the detonation wave passes each given point in the mesh. Usually the solid explosive before detonation is modeled as an elastic solid, while gasses released by the burn are modeled using the JWL EoS. To accomplish the appropriate energy release during the burn, the heat of formation of the solid explosive material is set such that the proper heat release is achieved.

The detonation front is computed by enforcing a burn fraction that is a function of the lighting time, t_1. The lighting time is the computed time that the detonation front will arrive at a given cell and is computed by

dividing the distance to the initiation point by the detonation velocity, D. The burn fraction, F, is zero if $t \le t_1$. When $t > t_1$, the burn fraction is defined by

$$F = \max\left(\frac{(t - t_1)D}{4\Delta}, \frac{1 - V}{1 - V_{CJ}} \right) \tag{10}$$

where t is the current simulation time, t_1 is the current cell lighting time, D is the detonation velocity, $V = \rho_0 / \rho$ is the relative volume, V_{CJ} is the relative volume at the Chapman-Jouguet conditions, and Δ is an estimated grid spacing for the mesh where the detonation front is propagating.

2.1.4 Numerical Considerations

When simulating multicomponent flows, it is possible to take a time-step such that the material in a cell is completely depleted, resulting in the time evolution of negative mass fractions of material. This non-physical circumstance is unacceptable because advancing the solution becomes nearly impossible. For first-order spatial approximations, depletion of the material from a cell is avoided if a time-step is employed that satisfies the stable CFL condition. However, when reconstructing higher-order mixture fractions, it is possible to deplete a material even though a much smaller time-step is used. To facilitate a second-order spatial reconstruction of species mass fractions, the mass fraction extrapolation is limited to ensure that a negative mass fraction is avoided (assuming a first-order upwind convection). While such limiting helps avoid the evolution of negative mass fractions, they can still evolve. Therefore, to provide an effective strategy that avoids negative mass fraction evolution in the time-stepping algorithm, the time-step is further limited to include the time required to deplete a cell of all species material using the first time-step residual. In practice, a CFL setting between 0.5 and 0.75 may still be required to avoid the evolution of negative mass fractions.

3.2 Coupling Loci/BLAST with LS-DYNA

3.2.1 Coupling Strategy

A two-way coupled, conformal blast-vehicle interaction analysis capability was developed utilizing Loci/BLAST and LS-DYNA. The loosely-coupled approach solves each set of governing equations within its own computational domain and interfaces the solutions at common boundaries. In this approach, the structural mesh is embedded in the fluid mesh in a conformal manner. That is, both the fluid mesh and the structures mesh share a common surface that deforms as prescribed by the LS-DYNA simulation. The surface mesh deformations predicted by LS-DYNA are projected into the fluid mesh enabling Loci/BLAST to simulate the fluid response to the structural deformation. The updated pressure loading on the LS-DYNA model is dynamically passed from Loci/BLAST thereby providing a two-way coupling capability between the two codes. The conformal approach does have limitations in that it is only applicable for problems with modest structural deformation and is not able to respond to topological change in the structure caused by fracture or fragmentation.

Once the structural deformations have been passed to the blast simulation, the conformal approach requires the fluid mesh to be modified to reflect these changes. A limiting feature of conformal approaches is the inability of the mesh movement strategy to adjust the volume grid in response to large surface deformations. In previous efforts, the widely used tension-torsion spring analogy was utilized. This approach suffers from the aforementioned bottleneck and thus has only a limited range in which the volume grid will remain valid or retain

sufficient quality.

The approach employed for the volume mesh deformation [19] is an interpolation-based method whereby the displacements at the boundary are interpolated into the volume. The unique feature of this approach is that the displacement field at each boundary point is decomposed into a displacement and rotation. The local rotation is included to reduce mesh shearing near the surface. These rotations are obtained by utilizing a least squares fitting method to find the closest rotation that matches the local displacement field. The interpolation method is based on a reciprocal distance weighted sum that is roughly analogous to an elastic model solved using a boundary element method. In order to obtain efficiency, a form of the fast multipole expansion approach is employed, whereby collections of points at a distance are approximated by a truncated expansion that represents the collection.

3.2.2 Load Transfer Algorithm

The coupling between the CSD software package LS-DYNA and the CFD-based blast simulation code Loci/BLAST was accomplished using the user defined loading feature available in LS-DYNA. Within the user-defined loading subroutine *loadud* a general interface was constructed. The interface performs all necessary mapping required between the fluid surfaces and structural model, and transfers load and displacements between the respective software packages in a conservative manner and thus provides all the capabilities required to perform two-way coupled, conformal blast-vehicle interaction.

Typically, load transfer schemes are based on projecting a fluid node onto the adjacent finite element face of the structural model. Ideally, the projection is defined such that the vector connecting the fluid node and the projected point is normal to the element face. This scheme is based on representing the fluid nodes and the adjacent element faces as rigid solid elements. Transferring the integrated loads from the fluid node to the projected point is then identical to connecting the two nodes with a rigid beam element. Since this is a statically determinate system, equilibrium equations are sufficient to transfer the load vector to a unique statically equivalent system. However, transferring the load vector from the projected point to the nodes of the structural element represents a statically indeterminate problem, and hence the use of the element shape functions to distribute these loads in a statically equivalent manner. It should be noted that since this transfer is statically indeterminate, it does not represent a unique set of nodal loads, only that the transfer is statically equivalent. Furthermore, this transfer is dependent on the location of the projected point, which is also selected and is not unique.

In order to uniquely transfer the integrated fluid forces to the nodes of the structural elements, the dependency on the projected point locations must be eliminated. Additionally, a statically equivalent force system must be defined for the statically indeterminate transfer. To accomplish this task, kinetics (equilibrium equations), kinematics, and constitutive relations must be utilized. The newly developed node-projection method constructs a solid element from the fluid node and the nodes of the adjacent structural element. The element equations contain the necessary information to enable the statically indeterminate transfer of the loads from the fluid node to the nodes of the structural element. As is well known, solid elements should typically be avoided for thin-walled structures, such as shells, since they are subject to locking. However, as will be shown, these concerns do not pose any difficulties as used in this formulation.

Given that the structural element face will be either triangular or quadrilateral, introduction of the fluid node will create a tetrahedral or a pyramidal element, respectively. Denoting the fluid node (apex node for the pyramidal element) as the last node in the element, node *n*, the element equations may be expressed as

$$\begin{bmatrix} [K_{1,1}] & \cdots & [K_{1,n-1}] & [K_{1,n}] \\ \vdots & \ddots & \vdots & \vdots \\ [K_{n-1,1}] & \cdots & [K_{n-1,n-1}] & [K_{n-1,n}] \\ [K_{n,1}] & \cdots & [K_{n,n-1}] & [K_{n,n}] \end{bmatrix} \begin{Bmatrix} \{\vec{\delta}_1\} \\ \vdots \\ \{\vec{\delta}_{n-1}\} \\ \{\vec{\delta}_n\} \end{Bmatrix} = \begin{Bmatrix} \{\vec{F}_1\} \\ \vdots \\ \{\vec{F}_{n-1}\} \\ \{\vec{F}_n\} \end{Bmatrix}, \tag{11}$$

where each $[K_{i,j}]$ represents a 3x3 submatrix within the element stiffness matrix, $\{\vec{\delta}\}$ are the nodal displacement components, and $\{\vec{F}\}$ the nodal force vectors. The complete element stiffness matrix may be evaluated using

$$[K] = \int_V [B]^T [D][B]\, dV\,, \tag{12}$$

where $[D]$ is the elastic matrix and $[B]$ is the strain-displacement matrix. To transfer the loads from the fluid node, the structural nodes may be considered to be supported, resulting in the displacement boundary conditions $\{\vec{\delta}_1\} = \cdots = \{\vec{\delta}_{n-1}\} = 0$. Solving this system for the unknown degrees-of-freedom, which represent the displacements at the fluid node, yields

$$\{\vec{\delta}_n\} = [K_{n,n}]^{-1} \{\vec{F}_n\} \tag{13}$$

Using Equation (11), the unknown reactions at the structural nodes may in turn be evaluated from

$$\{\vec{F}_j\} = [K_{j,n}]\{\vec{\delta}_n\} = [K_{j,n}][K_{n,n}]^{-1} \{\vec{F}_n\} \qquad j = 1,\ldots, m = n-1 \tag{14}$$

The above transfer provides a means of obtaining the statically equivalent loads to the statically indeterminate system. It is not dependent upon a projected point on the element and takes into account any mismatch or gaps between the fluid and structural surfaces. Furthermore, although the elastic matrix has been utilized, the product $[K_{j,n}][K_{n,n}]^{-1}$ for elastostatics is independent of the elastic modulus, but dependent on Poisson's ratio. For a perfectly rigid material Poisson's ratio is set to zero, and thus the force transfer is not a function of the material properties chosen for the element. Under these conditions, the 3x3 submatrices in Equation (14) are only dependent on the gradients of the shape functions.

When the fluid node lies in the plane of the element surface, or coincides with a structural node (i.e. a one-to-one match), the volume vanishes. For a tetrahedral element the integrand in the element stiffness matrix is constant, and in the product $[K_{j,n}][K_{n,n}]^{-1}$, the volume from each submatrix will cancel. Thus, degeneracy poses no difficulties. In the case of a pyramidal element, the element stiffness matrix must be numerically integrated. Using the isoparametric transformation to natural coordinates, the Cartesian derivatives require the inverse of the Jacobian, and in the case of degeneracy the Jacobian determinate vanishes. However, this situation can be avoided by determining the natural coordinates of the fluid node within a regular pyramid with the base being represented by the structural nodes. The natural coordinates of the fluid node for degeneracy will be in the same plane (of the master pyramid) as the base points. Subsequently, the product above may be numerically evaluated at these coordinates with a weight of unity. For validation purposes, numerous cases were simulated to test this algorithm, from one-to-one matched mesh transfers to arbitrary discretizations of the fluid and structural

surfaces. In all cases, load transfer and work done for time dependent simulations were conserved, with differences on the order of machine precision.

3.2.3 Inter-application Communication

To support coupling between LS-DYNA and Loci/BLAST, a simple socket protocol for communicating between the two applications was developed utilizing the POSIX standard API's for communicating using TCP/IP protocols. This socket library allows LS-DYNA and Loci/BLAST to exchange information whereby the two codes can run on either the same machines, or alternatively to two independent machines that can communicate using TCP/IP protocols (e.g. have an Internet connection between them). On the LS-DYNA side, a load subroutine is modified to call the socket library using an API that consists of two phases:

1. A registration phase which is initiated when LS-DYNA load subroutine is called for the first time. In the registration phase the load subroutine waits until Loci/BLAST connects with LS-DYNA.

2. Following the registration phase, the API provides a routine called fsi_interact_step where the load subroutine provides the current LS-DYNA simulation time, time-step, nodal displacements, velocities and accelerations. This interface passes the information (as needed) to the Loci/BLAST and then waits for LS-DYNA to return nodal forces to be applied during the next LS-DYNA time-step.

The Loci/BLAST side of the socket library provides facilities that are able to collect and distribute information to the parallel processes that are performing the simulation as well as coordinating the mapping between dissimilar meshes utilized on the structural and fluid sides of the problem. The API utilized on the Loci/BLAST side only communicates requested information through the socket, so that only the information that is needed to accomplish the transfer is communicated. In addition, the Loci/BLAST API supports sub-cycling whereby multiple fluid time-steps may be executed in order to integrate over a single LS-DYNA time-step. In this API, the Loci/BLAST application connects to the LS-DYNA application. The Loci/BLAST run is provided the machine Internet address of the LS-DYNA application. The socket library then uses this address to connect to the LS-DYNA run. Once the two applications are connected, the simulation proceeds automatically without further user intervention

4.0 RESULTS

4.1 Validation using DRDC Plate Data

Validation of the two-way coupled FSI algorithm was carried out using experimental and numerical data reported at the 7th International LS-DYNA Users Conference [20]. Data collected during field tests to study the effects of mine blasts on aluminum armor and RHA plates provides an opportunity to validate the FSI algorithm for a relatively simple geometry. Figure 1 depicts the arrangement and dimensions of the experimental apparatus. In the LS-DYNA model, a 31.75 mm target plate was described using the Johnson-Cook material properties for 5083-AL and was resolved with approximately 16K shell elements. The computational geometry used halfplane symmetry. The CFD mesh for target plate was discretized using roughly 1cm surface resolution. For the three-dimensional FSI simulation, Loci/BLAST was used with the HLLE inviscid flux, the nodal Barth flux limiter, and Runge-Kutta second-order time integration. A maximum CFL of 0.9 was implemented throughout the run. The cylindrical C4 charge with l/d=1/3 had a mass was 6 kg. The charge was buried at a depth of 5 cm in soil with a density of 2300 kg/m^3. It should be noted that detailed information about the composition of the soil was not provided.

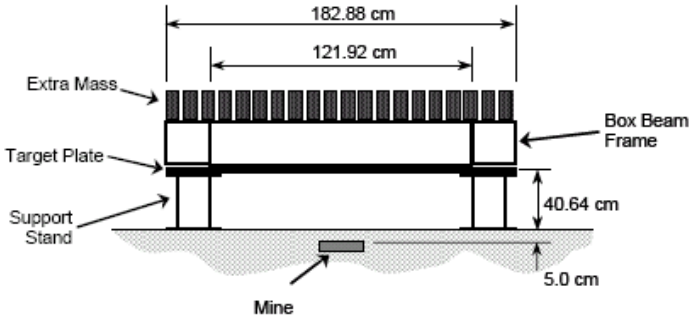

Figure 1: DRDC Experimental Set-up [20].

The solution process was initiated by performing an axisymmetric simulation of the charge detonation on a uniform mesh. The axisymmetric mesh had significantly higher resolution (approximately 0.5 mm spacing) than the fully three-dimensional mesh in the same region. The charge detonation was initiated at the center of the base of the charge and the axisymmetric simulation was executed for approximately 0.3 ms. The solution was then interpolated onto the computational domain employed for the fully three-dimensional simulation. The solution was continued for an additional 5 ms. The deformed plate geometries at 1 ms and 2 ms, as predicted by Loci/BLAST-LS-DYNA, are shown in Figures 2(a) and 2(b), respectively. Detailed comparisons with the experimental data and the Williams simulation data for the TACOM impulse loading model [20] are shown in Figures 3 and 4. Note the four experimental points for each station (distance from the center) are measured with respect to the "symmetry" plane axes and hence the variability shown indicates some slight asymmetry in the experiment. It should be noted that the Loci/BLAST data in the figures show the deformed positions of the plate at 5 ms and does not include the rigid body translation the entire plate was experiencing at that time. Overall, the agreement between the experimentally-observed deformation and the coupled Loci/BLAST-LS-DYNA predictions for this geometry is good. It should be noted that testing various solution procedures demonstrated the sensitivity of the maximum deformation of this geometry to soil density, charge weight, and DOB. This could explain the observed discrepancies since the precise composition of the soil was not reported.

4.2 Results for TARDEC Generic Hull

The coupled Loci/BLAST-LS-DYNA simulation capability was also tested on the simulation the detonation of a buried IED in close proximity to the TARDEC generic hull configuration [6]. Referring to Figure 5, a CFD mesh was built for the exterior space of the hull-surface elements. In Figure 5, the ground-plane is depicted as a magenta-colored mesh. In order to avoid nonphysical blast reflections, the soil (which is not shown in the figure) extended 3 meters below the ground-plane surface. A near-field transparent surface meshing box surrounded the vehicle to enable better control of the mesh points in the vicinity of the vehicle. Initially, an axisymmetric, high-resolution, buried-blast simulation was performed using the specifications for a 6 kg cylindrical (d/h = 3) charge of C4 buried approximately 5 cm below the surface in dry sand. For the axisymmetric simulation, a uniform mesh of 0.5 mm resolution was used. The axisymmetric solution was then interpolated onto the three-dimensional mesh and further evolution of the blast event was simulated.

The fully-coupled, three-dimensional simulations of the generic hull were run using 192 processors for Loci/BLAST and one processor for LS-DYNA. Due to a timestep disparity between the CSD and CFD simulations for this case, Loci/BLAST utilized several subcycle steps for the CFD part of the simulation. Also, due to the size of the CSD model, the Linux stack storage limit and memory allocation were increased for the LS-DYNA simulation. This three-dimensional run took roughly 15 wall-clock hours to complete. The snapshot

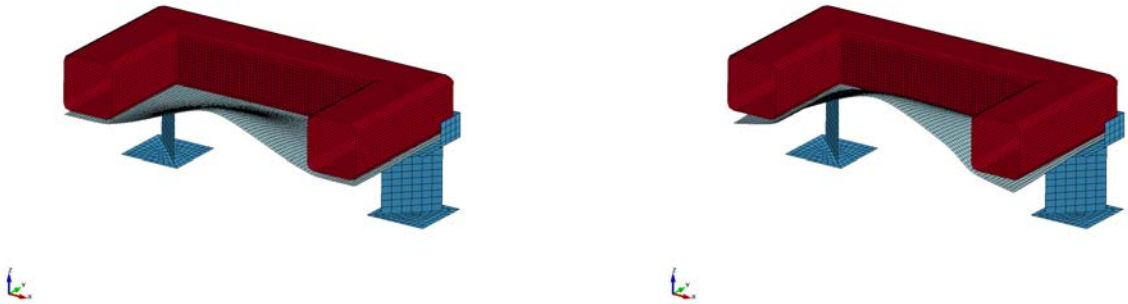

(a) deformed plate (1 ms) (b) deformed plate (2 ms)

Figure 2: Loci/BLAST–LS-DYNA Simulations for the DRDC Plate.

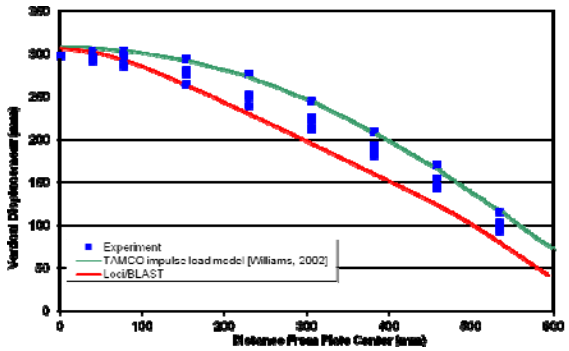

Figure 3: Displacement as a Function of Distance from Centerline.

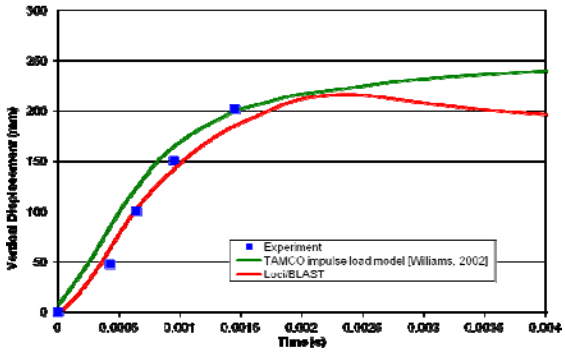

Figure 4: Time History of Displacement 30.5 cm from Plate Centerline.

shown in Figure 6 was generated after approximately 5 ms, with the isosurface of the 70% quartz (sand) volume fraction being displayed. Figure 7 shows an isosurface of pressure indicative of the blast front at approximately 5 ms. Most of the destructive forces of the blast occur in the first 2 ms of the simulation. Figure 8 shows the pressures on the surface of the hull 1ms after the initiation of the three-dimensional simulation; notice the buckling of the surface panels directly above the blast charge. The preceding images were from Loci/BLAST output data, additional structural data was obtained from LS-DYNA output. Figure 9 shows the hull surface, colored by stress, after 1 ms. Moving further into the interior of the structure, Figure 10 shows the structural frame supporting the outer skin and inner floor at approximately 1ms, again colored by stress.

The fully-coupled, three-dimensional simulations of the generic hull were run using 192 processors for Loci/BLAST and one processor for LS-DYNA. Due to a timestep disparity between the CSD and CFD simulations for this case, Loci/BLAST utilized several subcycle steps for the CFD part of the simulation. Also, due to the size of the CSD model, the Linux stack storage limit and memory allocation were increased for the LS-DYNA simulation. This three-dimensional run took roughly 15 wall-clock hours to complete. The snapshot shown in Figure 6 was generated after approximately 5 ms, with the isosurface of the 70% quartz (sand) volume fraction being displayed. Figure 7 shows an isosurface of pressure indicative of the blast front at approximately 5 ms. Most of the destructive forces of the blast occur in the first 2 ms of the simulation. Figure 8 shows the pressures on the surface of the hull 1ms after the initiation of the three-dimensional simulation; note the buckling

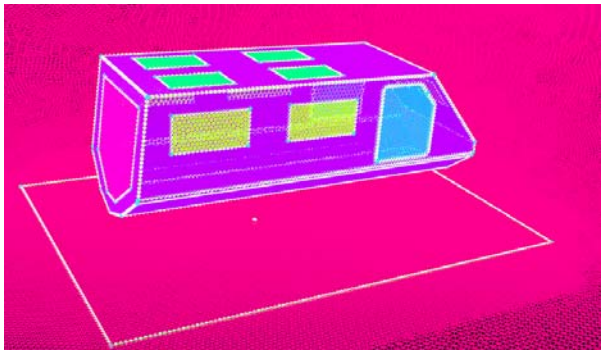

Figure 5: Unstructured CFD Mesh Used for Generic Hull.

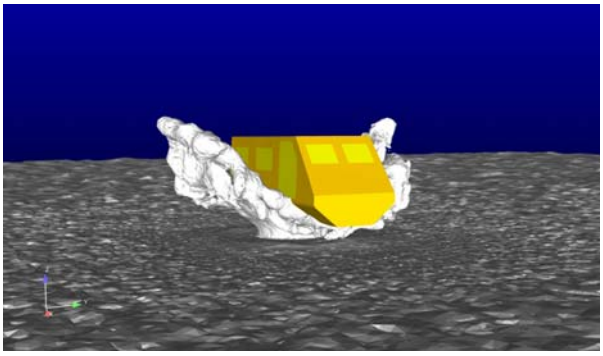

Figure 6: Quartz Cloud (70%Volume Fraction) at t=5 ms.

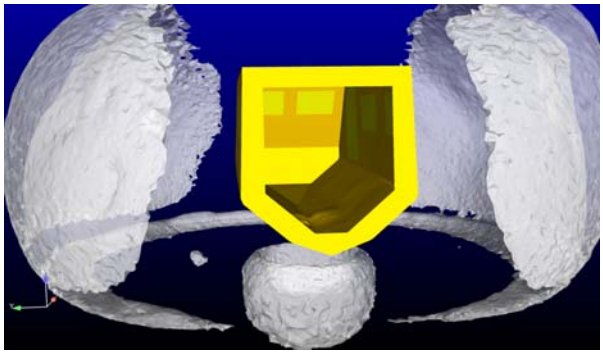

Figure 7: Representative Blast Front at t=5 ms.

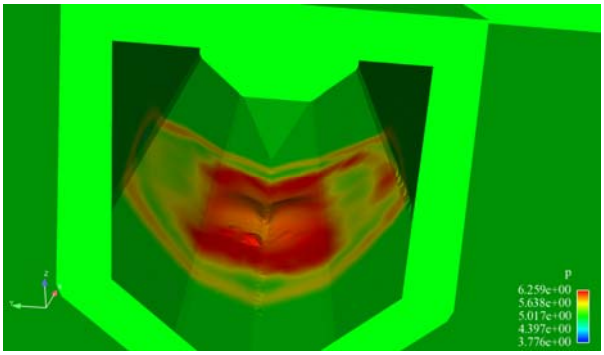

Figure 8: Log_{10} Pressure on Hull Surface at t=1 ms.

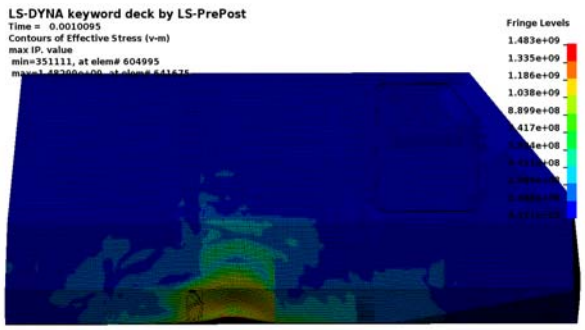

Figure 9: Generic Hull Outer Surface Stress Contours and Deflection.

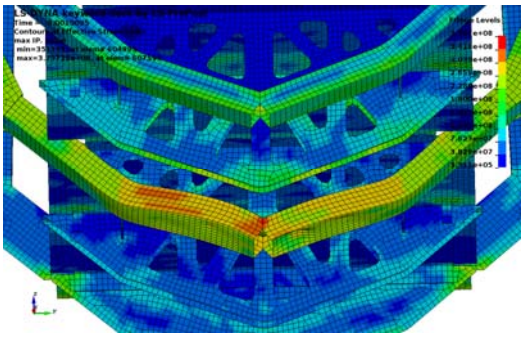

Figure 10: Generic Hull Stress and Deflection for Frame at t=1 ms.

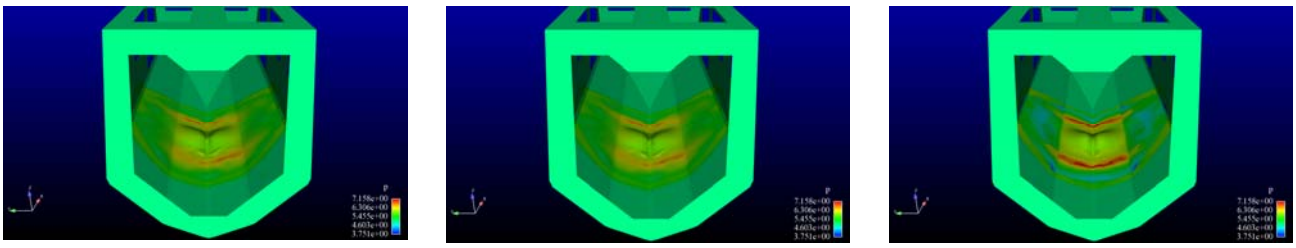

(a) 5 cm resolution (b) 2.5 cm resolution (c) 1.25 cm resolution

Figure 11: Log_{10} Pressure on Hull Surface at t=1 ms.

of the surface panels directly above the charge. The preceding images were generated using Loci/BLAST output data. Additional structural data was obtained from LS-DYNA output. Figure 9 shows the hull surface, colored by stress, after 1 ms. Moving further into the interior of the structure, Figure 10 shows the structural frame supporting the outer skin and inner floor at approximately 1ms, again colored by stress.

To further explore the coupled solution of the generic hull, a series of CFD grid refinements were undertaken. The grids will be referenced here based on the hull surface resolution, i.e., coarse (5 cm), medium (2.5 cm), and fine (1.25 cm). The soil model chosen was the *soil15* model. For this study, additional transparent surfaces were created underneath the vehicle to improve local resolution and reduce mesh density in regions known to be largely inactive over the simulation time. A marked increase in blast strength due to enhanced resolution is evident from the coarse to medium grids and less so from the medium to fine grids as illustrated in Figure 11, which shows pressure on the surface of the hull 1 ms after the initiation of the three-dimensional simulation. The increased CFD resolution results in an increase in load to the vehicle and hence greater deflections are seen on the vehicle surface as well as in the frame. From the hull, this greater load is then transferred to the internal frame of the vehicle. The deflection and stress distribution within the vehicle frame for the medium grid simulation are shown for 1 ms and 5 ms in Figures 12(a) and 12(b), respectively. In order to assess the differences in predicted deflections, two representative CSD nodes were selected and their deflections extracted. For reference, the locations of these nodes are shown in Figures 13 and 14. Figure 13 shows that the maximum skin-node deflection for the medium grid (approximately 80mm) is nearly 40% greater than the coarse grid (approximately 58 mm), while the fine grid further extends this surface deflection (approximately 94mm). Likewise, Figure 14 shows that the maximum frame-node deflection for the medium grid (approximately 43 mm) is again nearly 40% greater than the coarse grid (approximately 31 mm), while the fine grid only extends this deflection only slightly (approximately 47 mm). Note that for the fine grid simulation, after the blast wave had passed (approximately 1.8 ms), the CFD simulation ended and the LS-DYNA simulation was allowed to continue the structural response (with the unloaded nodes). The results, in particular those shown in Figure 13, suggest that an additional mesh refinement is needed.

4.0 SUMMARY AND CONCLUSIONS

The results shown here demonstrated that it is feasible to perform a two-way, conformal coupling between Loci/BLAST (Eulerian blast code) and LS-DYNA (Lagrangian structural dynamics code) to predict the effects of the detonation of a buried charge on a realistic ground vehicle configuration. While not applicable to problems with large structural change or vehicular topological change, e.g. fracture, the coupled technology provides a fully-conservative approach for predicting applied loads and damage to a vehicle.

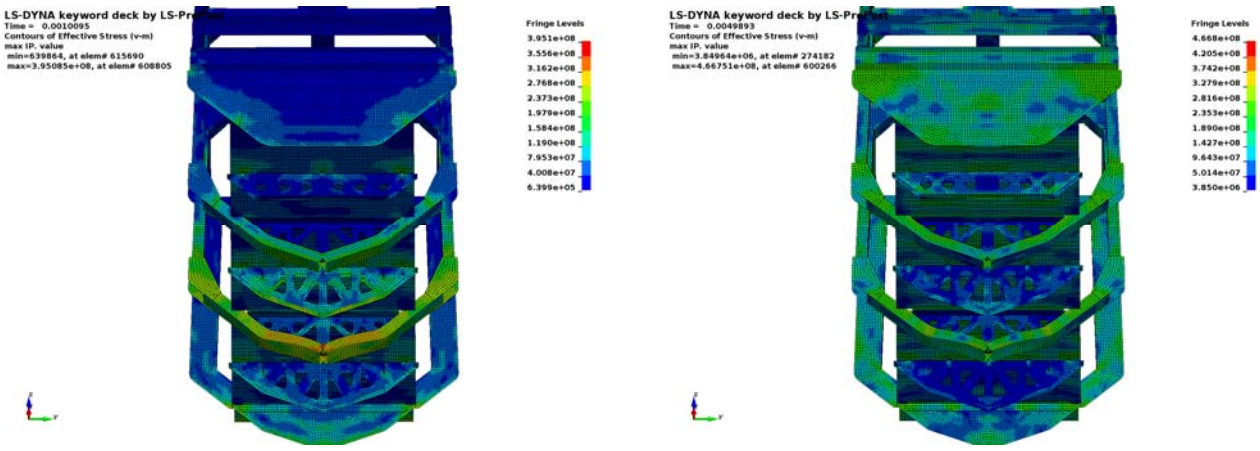

(a) frame configuration at t=1ms **(b) frame configuration at t=5ms**

Figure 12: Generic Hull Stress and Deflection Computed using the Medium Grid.

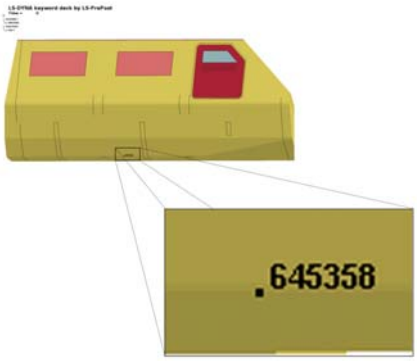

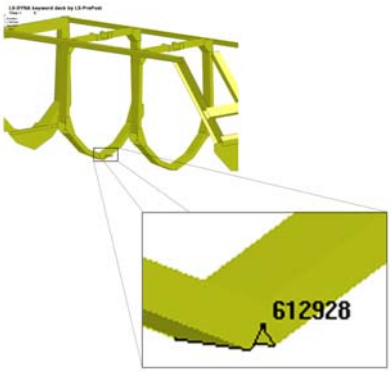

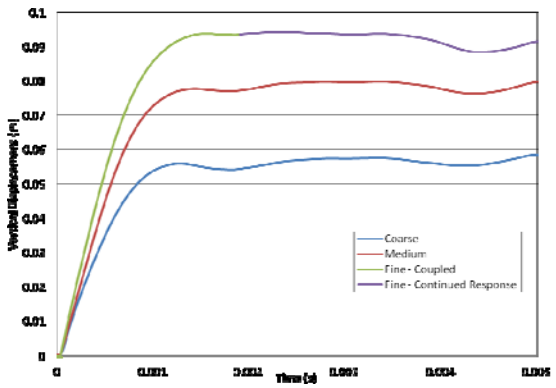

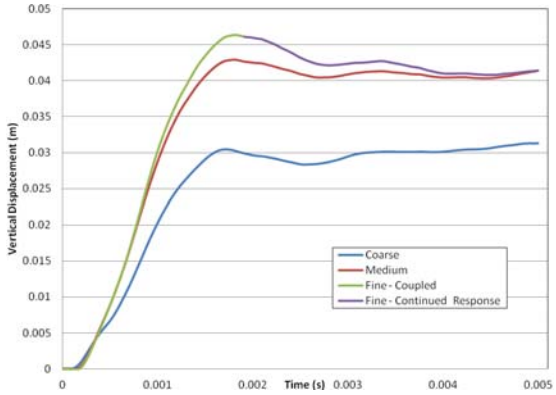

Figure 13: Deflection Time History Node 645358 (skin).

Figure 14: Deflection Time History Node 612928 (frame).

ACKNOWLEDGEMENTS

This material is based on work supported by the U.S. Army TACOM Life Cycle Command under Contract No. W56HZV-08-C-0236, through a subcontract with Mississippi State University, and was performed for the Simulation Based Reliability and Safety (SimBRS) research program. Any opinions, finding and conclusions or recommendations in this material are those of the author(s) and do not necessarily reflect the views of the U.S. Army TACOM Life Cycle Command.

REFERENCES

[1] Thompson, D., Luke, E., Newman III, J., Janus, J.M., Blades, E., Tong, X., Moore, C., and Kang, J. "Development of a Strategy for Simulating Blast-Vehicle Interactions," TACOM/TARDEC Report 21200RC, 2010.

[2] Thompson, D., Janus, J.M., Luke, E., Moore, E., Remotigue, M., Tong, X.L., Weed, R., and Ivancic, P. "Enhanced Simulation of Blast-Vehicle Interactions using Loci/BLAST and LS-DYNA," Final Report for SimBRS WD 0034, Contract No. W56HZV-08-C-0236, 2012.

[3] Thompson, D., Luke, E., Remotigue, M., Janus, J.M., Wang, W., Collins, W., Arnoldus, W., Trcalek, M., Weed, R., Moore, C., Tong, X., Britt, J.R., Bessette, G., and Hyde, D. "Multi-Fidelity Tools for Blast Analysis in Urban Environments," SERRI Report 90028-01, Oak Ridge National Laboratory, 2012.

[4] LS-DYNA User Manual, Version 971, Livermore Software Technology Corporation, 2007.

[5] Williams, K., McClennan, S., Durocher, R, St-Jean, B., Trembelay, J., "Validation of a Loading Model for Simulating Blast Mine Effects on Armoured Vehicles," 7th International LS-DYNA Users Conference, Detroit, MI, 2002.

[6] Dooge, D., Dwarampudi, R., Schaffner, G., Miller, A., Thyagarajan, R., Vunnam, M., and Babu, V. "Evolution of Occupant Survivability Simulation Framework Using FEM-SPH Coupling," NDIA Ground Vehicle System Engineering and Technology Symposium (GVSETS), MSTV Mini-Symposium Paper, August 9-11, Dearborn, MI, 2011.

[7] Tai, C. H., Liew, K. M., and Zhao, Y. "Numerical simulation of 3d fluid-structure interaction flow using an immersed object method with overlapping grids," Computers & Structures, 85(11-14):749–762, 2007.

[8] Silver, P.L. "Blast overpressure measurement for cfd model validation in the development of large caliber gun systems," In 41st Annual Armament Systems: Guns and Missile Systems Conference and Exhibition, 2006.

[9] Kim, D.K. and Han, J.H. "Establishment of gun blast wave model and structural analysis for blast load,"

Journal of Aircraft, 43(4):1159–1168, 2006.

[10] Lottati, I., Eidelman, S., Dillon, J., Sergi, S., and Sousk, S. "Design of blast deflectors for a mine resistant vehicle by cfd/csd simulations," ASME Publications Pressure Vessels and Piping Division, Structures under Extreme Loading Conditions, 325:51–61, 1996.

[11] Fairlie, G. and Bergeron, D. "Numerical simulation of mine blast loading on structures," In 17th Military Aspects of Blast Symposium, Las Vegas, Nevada, 2002.

[12] Grujicic, M., Pandurangan, B., Haque, I., Cheeseman, B., Roy, W., and Skaggs, R. "Computational analysis of mine blast on a commercial vehicle structure," Multidiscipline Modeling in Materials and Structures, 3(4):431–460, 2007.

[13] Grujicic, M., Bell, W.C., Marvi, H., Haque, I., Cheeseman, B.A., Roy, W.N., and Skaggs, R.R. "A computational analysis of survivability of a pick-up truck subjected to mine detonation loads," Multidiscipline Modeling in Materials and Structures, 7(4):386-423, 2011.

[14] Fallet, R. "Mine explosion and blast effect on vehicle analysis of the potential damage on passengers," In 2nd European HyperWorks Technology Conference, Strasbourg, 2008.

[15] Luke, E., and Cinnella, P. "Numerical simulations of mixtures of fluids using upwind algorithms," Computers and Fluids, 36:1547-1566, 2007.

[16] Lee, E.L., and Tarver, CM. "Phenomenological model of shock initiation in heterogeneous explosives," Physics of Fluids, 23(12): 2362-2372, 1980.

[17] Luke, E., and George, T. "Loci: A rule-based framework for parallel multidisciplinary simulation synthesis," Journal of Functional Programming 15(3):477-502, 2005.

[18] Li, Y.-H., "Equation of State for Water and Sea Water," Journal of Geophysical Research, 72(10):2665-2678.

[19] Luke, E., Collins, E., and Blades, E. "A fast mesh deformation method using explicit interpolation," Journal of Computational Physics. 231(2):586–601.

[20] Westline, P. "The impulse imparted to targets by the detonation of land mines," The Shock and Vibration Bulletin. No. 42, 1972.